Oceanic gateways in Antarctica - Impact of relative sea-level change on sub-shelf melt

Moritz Kreuzer[1,2], Torsten Albrecht[1], Lena Nicola[1,2], Ronja Reese[3,1], and Ricarda Winkelmann[1,2]

[1] Potsdam Institute for Climate Impact Research (PIK), Member of the Leibniz Association, P.O. Box 601203, D-14412 Potsdam, Germany

[2] University of Potsdam, Institute of Physics and Astronomy, Karl-Liebknecht-Str. 24-25, D-14476 Potsdam, Germany

[3] Department of Geography and Environmental Sciences, Northumbria University, Newcastle, UK

Correspondence: Moritz Kreuzer (kreuzer@pik-potsdam.de)

Abstract. Relative sea level (local water depth) on the Antarctic continental shelf is changing by the complex interplay of processes associated with Glacial Isostatic Adjustment (GIA). This involves near-field visco-elastic bedrock displacement and self-gravitational effects in response to changes in Antarctic ice load, but also far-field interhemispheric effects on the sea-level pattern. On glacial time scales, these changes can be in the order of several hundred meters, modulating the access of ocean water masses at different depths to Antarctic grounding lines. Our study shows, that due to strong vertical gradients in ocean temperature and salinity at the continental shelf margin, basal melt rates of ice shelves can change significantly just by variations in relative sea level alone. Based on coupled ice sheet – GIA model experiments and the analysis of topographic features such as troughs and sills that regulate the access of open ocean water masses onto the continental shelf (oceanic gateways), we derive maximum estimates of Antarctic basal melt rate changes, solely driven by relative sea-level variations. Under Last Glacial Maximum sea-level conditions, this effect would lead to a substantial decrease of present-day sub-shelf melt rates in East Antarctica, while the strong subsidence of bedrock in West Antarctica can lead up to a doubling of basal melt rates. For a hypothetical globally ice-free sea-level scenario, which would lead to a global mean (barystatic) sea-level rise of around +70 m, sub-shelf melt rates for a present-day ice sheet geometry can more than double in East Antarctica, but can also decrease substantially, where bedrock uplift dominates. Also for projected sea-level changes at the year 2300 we find maximum possible changes of $\pm 20\,\%$ in sub-shelf melt rates, as a consequence of relative sea-level changes only.

1 Introduction

Global-mean sea level (GMSL) varies on glacial-interglacial time scales in the order of 100 m depending on the density of ocean water (steric effects) and the total ocean area, which is determined by the mass redistribution between ocean and land (e.g. by ice sheet changes; Miller et al., 2020; Horwath et al., 2022). The latter component is also referred to as *barystatic sea-level change* (Gregory et al., 2019), and is the dominant component of GMSL changes since the Last Glacial Maximum (LGM, ca. 21 kyr BP; Gebbie, 2020). The global distribution of the sea level aligns according to an equipotential surface, also called the *geoid* (Gregory et al., 2019), which is determined by the gravity field of ice, water and the Earth's mantle material, with a feedback on Earth's rotation. Variations of sea-level height through ocean currents and winds are not covered by the

geoid definition. The *relative sea level* (RSL) is the depth of the water column, hence the vertical distance between the geoid and the ocean bathymetry (or when negative, the land surface elevation above the geoid), and it can change through several processes:

1. *Changes in ice masses* affect the volume and area of the global ocean, leading to a globally distributed, barystatic shift of the geoid height.

2. The mass redistribution between ice and ocean also affects the Earth's *rotational* axis, such that the global sea-level pattern adjusts to the change in centrifugal acceleration.

3. The *gravitational* force exerted by ice masses on the surrounding ocean masses leads to variations in local geoid height near ice sheets when there is a gain or loss of ice mass.

4. Changes in load have *deformational* (visco-elastic) effects on the solid Earth, leading to subsidence or uplift of the underlying bedrock topography. This causes a horizontal flux of mantle material as well as an elastic response of the lithosphere. The reverse signal in RSL, which occurs in the vicinity with smaller magnitude is called a 'forebulge'. Depending on the local mantle viscosity and lithosphere thickness, this visco-elastic process can induce vertical changes of hundreds of meters.

These mechanisms act on different spatial and temporal scales, i.e. almost instantaneous in case of of rotational and gravitational effects, whereas bedrock deformation can take several millennia to unfold. All of the mentioned mechanisms are covered by the *Glacial Isostatic Adjustment* theory (GIA; Farrell and Clark, 1976; Whitehouse, 2018). Global mean sea level is also influenced by thermosteric effects through changes in ocean water temperature, but this effect is comparably small on glacial time scales.

During the Last Glacial Maximum, GMSL was about 125–134 m lower than today, mainly due to the greater extent of northern hemisphere ice sheets (Yokoyama et al., 2018; Lambeck et al., 2014). Grounded ice in Antarctica reached close to the continental-shelf break in many locations during LGM (Bentley et al., 2014) and holding up to 20 m sea-level equivalent more ice, according to the literature review in Albrecht et al. (2020b, Fig. 11b). Today's configuration of the Antarctic Ice Sheet (AIS) still holds enough ice to raise GMSL by approx. 58 m if melted completely (neglecting isostatic or thermal effects; Morlighem et al., 2020). Considering all land-based ice on Earth, including the Greenland Ice Sheet and mountain glaciers, this number increases to approx. 66 m (IPCC AR6 WG1 Ch. 2.3.3.3, Gulev et al., 2021).

While Antarctic ice mass changes have been small in the Late Holocene (approx. last 4000 years, Jones et al., 2022), the AIS is losing mass at an increasing rate in the last decades (Shepherd et al., 2012; Rignot et al., 2019; Otosaka et al., 2023). Due to ongoing atmospheric and ocean warming, it is projected that Antarctica loses up to 3.13 m of sea-level equivalent ice volume by 2300 under a high-emission scenario (IPCC AR6 WG1 Ch. 9.6.3.5, Fox-Kemper et al., 2021). When considering the long-term stability of the ice sheet, Garbe et al. (2020) find that due to several feedback mechanisms, the AIS is bound to

become ice-free at warming greater than $10\,°C$ above pre-industrial levels.

In order to assess the stability and long-term behaviour of ice sheets, interactions with the solid Earth and sea level are relevant as GIA responses can have major feedbacks on ice dynamics (Whitehouse et al., 2019). Albrecht et al. (2023, in prep.), for instance, use a globally consistent coupled ice sheet – GIA model framework and find that ice retreat can be significantly slowed down when isostatic rebound is included, in particular when considering a weak Earth structure with low mantle viscosity and thin lithosphere, as reconstructions suggest for the West Antarctic plate (Barletta et al., 2018). Coupled ice sheet – GIA models exist in different modes of complexity, e.g. with regional setups (Coulon et al., 2021; Zeitz et al., 2022), 1-dimensional Earth structure (Pollard et al., 2017; Gomez et al., 2020) or globally 3-dimensional, which are just becoming available as in van Calcar et al. (2023) and Albrecht et al. (in prep. 2023).

For ice-sheet simulations over long time scales, such as glacial cycles, climatic boundary conditions as ocean and atmospheric temperature have to be parameterized in an appropriate way. Albrecht et al. (2020a) use a temperature-index method and linear response functions to scale present-day ocean temperature observations on the continental shelf, which is the shallow ocean area surrounding the Antarctic Ice Sheet, with climatic variations derived from ice core data. A similar approach is taken by Chandler et al. (2023, in discus.), which has been successfully tested against paleo reconstructions (Chandler and Langebroek, 2023, in discus.). Melting of ice shelves, the floating extensions of the marine ice sheets, is highly sensitive to changes in ocean temperatures on the continental shelf, especially when warm water masses intrude into the ice-shelf cavities at depth (Hellmer et al., 2012; Pritchard et al., 2012; Rintoul et al., 2016). Sub-shelf melt rates are generally highest close to the grounding line, where grounded ice becomes afloat (Rydt and Gudmundsson, 2016). The grounding line position is determined by the RSL via the floatation condition. Hence, changes in RSL can affect the grounding line position and the ice-sheet dynamics. In fact, changes in RSL can also influence the ocean forcing directly, which we discuss in the following:

As (positive values of) RSL indicate the local water column depth, changes of RSL can be interpreted as a negative displacement of bedrock topography. From an ice-sheet perspective the local sea level thus remains at the same reference elevation ($z = 0$). The change in bedrock provides potential access to the continental shelf for water masses from different depths, assuming that bathymetry primarily controls flow. The upper layers of the Southern Ocean (approx. upper $600\,m$) show a strong increase of potential temperature with depth of about $+0.5\,°C$ per 100 meters on average (see Fig. S4 in the Supplement). This *thermocline layer* is characterised by the transition between cold and fresh surface waters and warmer, saltier Circumpolar Deep Water (CDW). The typical depth of the continental shelf around Antarctica (approx. $500\,m$) is in the range of the thermocline layer, such that small RSL changes can have a comparably large effect on the available ocean temperature and heat on the continental shelf, assuming no changes in flow pattern resulting from RSL changes. As depicted in Fig. 1, sea-level changes in the order of 100 meters can have significant impacts on the heat available for melting at the ice-shelf base, even with no further climatic temperature changes or grounding line migration considered.

Furthermore, the pattern of RSL changes is highly dependent on the local GIA response to ice dynamics. Visco-elastic vertical displacement of bedrock as a consequence of a changing ice load can outweigh the barystatic sea-level signal and lead
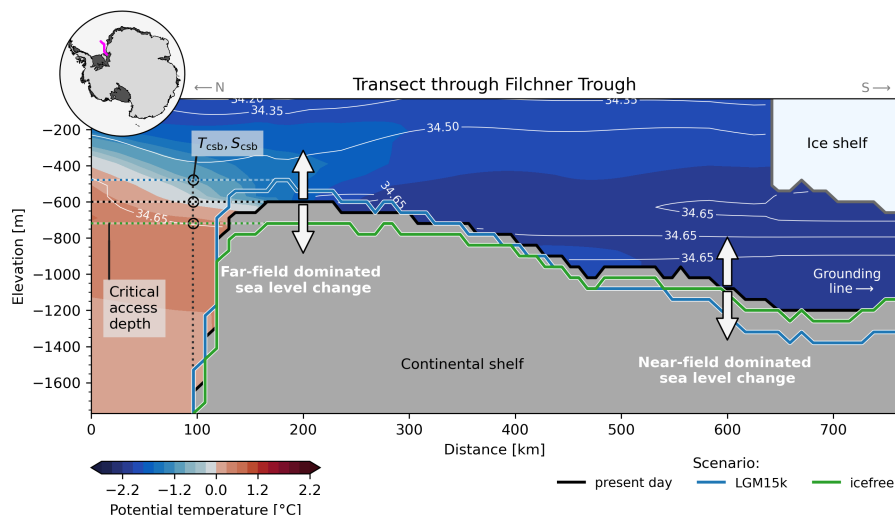
Figure 1. Transect through Filchner Trough showing relevant terms and concepts used in this study. The sill north of Filchner–Ronne Ice Shelf determines the critical access depth of the basin, indicated by dashed horizontal lines. Variations of the sill depth can occur in response to barystatic and far-field sea-level changes while the bathymetry within the ice-shelf cavity is mainly influenced by the near-field effects from GIA, which can induce an additional forbuldge effect on sill depth. To assess the potential impact of those changes on sub-shelf melt, temperature and salinity (the latter indicated as white contour lines in unit psu) estimates from Jourdain et al. (2020) are evaluated at the critical access depth near the continental-shelf break, marked as T_{csb}, S_{csb}. Magenta line in inlet map shows transect location.

to several hundreds of meter change in RSL, on glacial time scales. In a related study, Nicola et al. (2023b, subm.) show that bathymetry generally plays a crucial role in the interaction between the AIS and the surrounding ocean: topographic features such as troughs and sills act as *oceanic gateways* as they provide or block access of warm CDW into the ice-shelf cavities towards deep-lying grounding lines. A changing topography through regionally varying patterns of relative sea level thus has

95   the potential to strongly influence basal melting in the ice-shelf cavities.

In this study, we investigate the potential influence of relative sea-level changes on Antarctic ice-shelf basal melt rates in 19 individual basins around Antarctica, due to deformational, rotational or gravitational effects of GIA in response to the redistribution of masses between ice and ocean. To our knowledge this effect has not been quantified so far. We therefore

100   derive estimates for the maximum impact of this effect, based on upper limit scenarios, but also asses the impact on time scales of the upcoming centuries. We explain the methodology of our analysis in Sect. 2, present the results in Sect. 3 and end with a discussion (Sect. 4) and conclusion of our results (Sect. 5).

2 Methods

This section describes the methods, scenarios and workflow we use to derive ice-shelf basal melt rate estimates from relative
sea-level changes.

To derive upper limit estimates, the analysis is based on two 'end-of-the-spectrum' scenarios: (1) a global land-ice distribution during the Last Glacial Maximum with a global mean (barystatic) sea level approx. 93 m lower than today, and (2) a configuration with all continental ice masses transformed into liquid water (GMSL ≈ +70 m). In order to assess also near-future impacts, we add another scenario (3) based on a projection following the ISMIP6 Antarctica extensions until the year 2300 with a high emission scenario (SSP5-8.5). In the following we will refer to these scenarios as *LGM15k*, *icefree* and *yr2300*, which are described further below (Sec. 2.5).

To estimate sub-shelf melt rate changes for the scenarios mentioned above, we follow these steps:

1. Compute relative sea-level changes with coupled ice sheet – GIA simulations.

2. Identify critical depths informed by relative sea-level changes to determine open ocean access to ice-sheet grounding lines.

3. Calculate ocean state changes at the continental-shelf break due to vertical displacement of critical access depths.

4. Compute diagnostic changes in ice-shelf basal melt rates with an ice-sheet model.

The computation of RSL changes involves dynamic ice-sheet changes, while the rest of the analysis relies on a static, present-day configuration of the AIS and the surrounding ocean. Reasons and implications of this are further discussed in Sect. 4. In the following, we explain the methodology of each step in more detail.

2.1 Computation of relative sea-level changes

We simulate RSL changes using the coupled ice sheet – GIA model framework PISM-VILMA as described in Albrecht et al. (2023, in prep.). The Parallel Ice Sheet Model (PISM; https://www.pism.io; Bueler and Brown, 2009; Winkelmann et al., 2011), an open-source model which simulates ice sheets and ice shelves, is used to compute the transient evolution of the Antarctic Ice Sheet under external climatic boundary forcings. It is interactively coupled to the VIscoelastic Lithosphere and MAntle model (VILMA; Klemann et al., 2008; Martinec et al., 2018), which calculates the solid Earth and sea-level response to changes in ice loading based on a 3D Earth structure (Bagge et al., 2021). VILMA solves self-consistently the global sea-level equation, which yields a sea-level fingerprint in response to the redistribution of water masses between ice sheets and ocean, as well as a result of rotational and gravitational feedbacks. The simulations use a coupling interval of 100 years to update changes of ice load and bed topography between PISM and VILMA. For the ice loading history of the northern hemisphere over the last glacial cycle we use the ICE-6G_C reconstruction (Stuhne and Peltier, 2015). A detailed description of the coupled PISM-

VILMA framework and sensitivities to coupling parameter, resolution and Earth structures is given in Albrecht et al. (2023, in prep.).

We interpret the computed sea-level changes relative to the geoid as negative shifts in bathymetry and update the present-day topography of the BedMachine Antarctica (v3) dataset (Morlighem, 2022; Morlighem et al., 2020), conservatively regridded to $8\,\mathrm{km}$ horizontal resolution, for all scenarios accordingly.

2.2 Identification of critical access depths

In order to evaluate how the altered bathymetry changes the water masses that have access onto the continental shelf and into ice-shelf cavities, we make use of the approach developed in Nicola et al. (2023b, subm.). Therein, *oceanic gateways* are defined as the deepest possible entry point of open ocean water to the grounding lines of the Antarctic Ice Sheet. First, we compute *access depth* maps, which indicate for every location on the continental shelf, the deepest possible topographic connection to the open ocean. This is implemented with a successive flood-fill algorithm, which starts in the Southern Ocean, far from the continental-shelf break and iteratively propagates to all adjacent grid points that have the same or lower bathymetry. We perform this analysis on $8\,\mathrm{km}$ horizontal bathymetry resolution and iterate vertically in steps of $1\,\mathrm{m}$. Then, we evaluate the resulting 2-dimensional field of access depths at the present-day grounding line position for all scenarios. This results in *'critical access depth'* scalars $d_c(s,b,g)$, which indicates the lowest possible connection between the open ocean and the deepest grounding line fraction g, ranging from $10\,\%$ to $90\,\%$, varied in steps of $5\,\%$. We calculate critical access depths for each of the scenarios s described above and for each of the 19 basins b as defined in Zwally et al. (2012), with some of the basins being merged as in Reese et al. (2018).

The deepest lying grounding line sectors typically feature high ice velocities, and thereby the biggest ice fluxes across the grounding line, see also Nicola et al. (2023b, subm.). However, it is difficult to define a uniform threshold of relevant grounding line coverage, where a change in critical access depth is most relevant, due to the great heterogeneity between the basins. We therefore assess changes in critical access depths across the full spectrum between $10\,\%$ and $90\,\%$.

2.3 Calculation of marginal ocean properties

We assume, that a shift in critical access depths gives water masses from varying depths potential access onto the continental shelf and to the grounding lines. In order to assess the induced changes, we evaluate the vertical column of ocean temperature (T_{csb}) and salinity (S_{csb}) at the continental-shelf break (horizontal position where topography follows $z = -1800\,\mathrm{m}$ isobath). We define the mean continental-shelf temperature $\overline{T_{\mathrm{csb}}}(s,b,g)$ as the horizontal average of T_{csb} in basin b at critical access depth $d_c(s,b,g)$, similar to Nicola et al. (2023b, subm.). We then use the difference $\Delta\overline{T_{\mathrm{csb}}}(s,b,g)$ to the present-day control conditions for each scenario (see Eq. 1) to modify the ocean forcing input for calculating basal melt rate changes within the ice-sheet model, as described in the next section.

$$\Delta\overline{T_{\mathrm{csb}}}(s,b,g) = \overline{T_{\mathrm{csb}}}(s,b,g) - \overline{T_{\mathrm{csb}}}(s = \text{present-day}, b, g) \tag{1}$$

165   Salinity anomalies $\Delta\overline{S_{csb}}(s,b,g)$ are computed accordingly. As in Nicola et al. (2023b, subm.), we use the ISMIP6 clima-
tology dataset (Jourdain et al., 2020), which contains potential temperature and practical salinity data points averaged over the
period 1995-2017, available at a 8 km x 8 km horizontal and 60 m vertical resolution. To acquire ocean properties between
discrete vertical data layers, we utilize linear interpolation along the vertical axis.

2.4   Computation of basal melt in ice-shelf cavities

170   For computing basal melt rates we use the Potsdam Ice shelf Cavity mOdule (PICO) as implemented in the ice-sheet model
PISM (Reese et al., 2018). PICO parameterizes the vertical overturning circulation in ice-shelf cavities driven by melt-induced
buoyancy fluxes, extending the box model by Olbers and Hellmer (2010) to two horizontal dimensions. The module takes
ocean temperature and salinity at continental shelf depth as input, averaged horizontally per basin.

    As a baseline, we use PICO parameters from Reese et al. (2023, AIS1) including their ocean forcing data, which is based
175   on Schmidtko et al. (2014). The parameters are $C = 3.0 \, \mathrm{Sv \, m^3 \, kg^{-1}}$ for the strength of the vertical overturning circulation and
the heat exchange coefficient $\gamma_T^* = 7 \times 10^{-5} \, \mathrm{m \, s^{-1}}$. The tuning of Reese et al. (2023) optimises for the best fit of present-day
observed melt rates as well as melt-rate sensitivities to thermal forcing. For each scenario s and grounding line accessibility g,
we then compute adjusted sub-shelf melt rates $\dot{m}(s,b,g)$ by adding the computed ocean forcing anomalies $\Delta\overline{T_{csb}}(s,b,g)$ and
$\Delta\overline{S_{csb}}(s,b,g)$ to each corresponding basin b in the baseline forcing.

180   To initialise PISM, we use ice geometry (thickness) and bedrock topography of BedMachine v3 (Morlighem et al., 2020),
regridded to a horizontal resolution of 4 km.

2.5   Scenarios

This subsection provides more information about the scenarios used to compute RSL changes with the coupled ice sheet – GIA
model (step 1).

185   The *LGM15k* scenario is preceded by a coupled ice sheet – GIA model spinup of two glacial cycles with prescribed northern
hemisphere ice load history from the ICE-6G_C reconstruction (Stuhne and Peltier, 2015) to account for the memory effects of
Antarctic Ice Sheet behaviour. The methodology is further described in Albrecht et al. (2023, in prep.). We follow similar AIS
climate forcing and initialisiation as in Albrecht et al. (2020a). During the coupled simulation, the maximum AIS extent during
the last glacial period is reached at around 15 kyr BP, which is approx. 11 thousand years later than in the northern hemisphere
190   (26 kyr BP, see Fig. S1). This delay agrees well with literature (West Antarctic LGM 4.5-12 kyr later than global LGM sea-
level lowstand in Clark et al., 2009) and the ICE-6G_C reconstruction. In our simulation, GMSL was approx. 93 m lower
than today during that period. We derive relative sea-level changes for this scenario as the difference between the maximum
Antarctic ice extent and present-day. If not stated otherwise, we will use the term Last Glacial Maximum (LGM) with respect
to the Antarctic Ice Sheet in the following.

195   In the *icefree* scenario, the solid Earth response to a removal of all present-day ice load is computed. Continental ice masses
are redistributed as liquid water and added to the ocean mass, which leads to a GMSL rise of approx. 70 m in our simulation.

The simulation period spans 86 kyr into the future to account for long-term solid Earth response also in regions with strong Earth structure featuring high mantle viscosities and a thick lithosphere.

For the *yr2300* scenario, we start the coupled ice sheet – GIA simulations in year 1850 with a historical spin-up phase, where we observe plausible RSL change rates as observed by GNSS measurements. Then, from present-day onwards, the ice-sheet climate forcing follows the ISMIP6 2300 extension protocol using a SSP5-8.5 realisation of CESM2 (AE04, The ISMIP6 2300 extension authors, 2022). We use the best scoring member of ice-sheet initialisation ensemble from Reese et al. (2023, AIS1) as setup for the Antarctic Ice Sheet. While the climate forcing reflects an upper end estimate, the dynamic ice-sheet response does not include structural uncertainties of ice sheet behaviour such as the Marine Ice Cliff Instability (MICI), which can potentially increase Antarctic ice loss by a multiple (IPCC AR6 WG1 Ch. 9.6.3.5, Fox-Kemper et al., 2021). To include also non-Antarctic cryospheric changes and reflect redistributions in the global water budget, we add a uniform GMSL contribution of 3.68 m on the relative sea-level changes computed by PISM-VILMA, which is composed from upper end (83th percentile) IPCC estimates for the year 2300 under SSP5-8.5 forcing: the contributions are 1.75 m from the Greenland Ice Sheet, 0.32 m from glaciers, 0.10 m from land-water storage and 1.51 m from thermal expansion (IPCC AR6 WG1 Ch. 9.6.3.5, Fox-Kemper et al., 2021, Table 9.11). By adding a uniform, global mean sea-level offset to relative sea-level changes computed by PISM-VILMA we make the assumption, that regional variations from the global mean around Antarctica, e.g. induced by gravitational or rotational effects in response to these contributions (with origin mostly on the northern hemisphere), are small and not relevant on the scale of our assessment, which uses a vertical resolution of 1 meter to identify critical access depths from topography.

3 Results

In this section we describe the results of our analysis investigating the impact of relative sea-level change on Antarctic ice-shelf basal melt rates. First, we describe RSL changes for the *LGM15k* and *icefree* scenarios from the coupled ice sheet – GIA simulations. The derived changes in critical access depths are described thereafter, before we assess the impact on ocean temperature and salinity conditions which drive the changes in basal melting. Subsequently, we take a look into policy relevant time scales and present results for the *yr2300* scenario.

3.1 Changes in relative sea level

Our *LGM15k* simulation shows a maximum grounding line extent close to the continental-shelf break in almost all locations and increased ice thickness (up to +3000 m larger than today) especially in the marine basins, where today's largest ice-shelves are located, the Filchner–Ronne (basin 1) and Ross (basin 12) as well as in large portions of the West Antarctic Ice Sheet (basins 13–16). To a lesser extent this is also the case for the Antarctic Peninsula (basins 17–19) and the edges of East Antarctica (see Fig. S2). The interior of the East Antarctic Ice Sheet, however, shows a slight decrease of thickness during *LGM15k* (up to -140 m locally) due to less snowfall with colder surface temperature forcing (Nicola et al., 2023a). The additional ice load
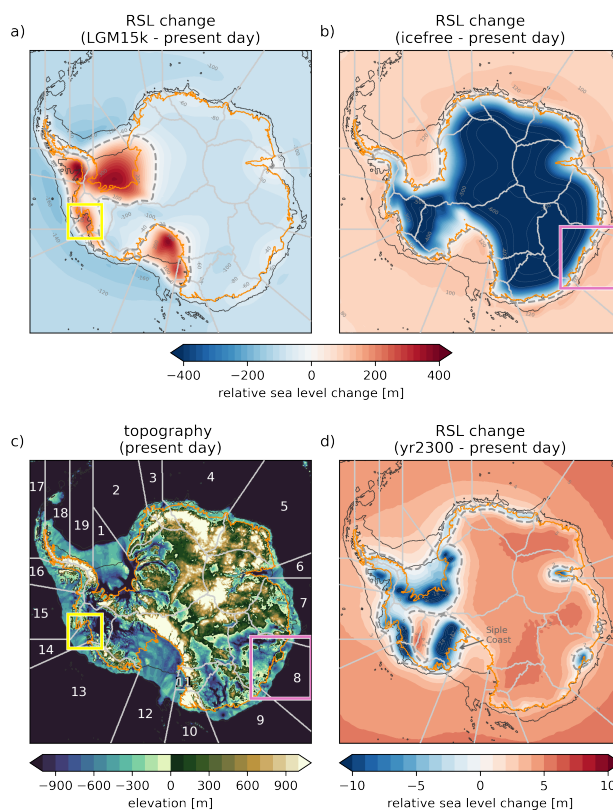
Figure 2. Changes in relative sea level for different scenarios and present-day topography. Changes in relative sea level are shown for *LGM15k* (a), *icefree* (b) and *yr2300* (d) scenarios. The transition between positive and negative relative sea-level changes is indicated by thick dashed grey contour lines. Horizontally adjusted grounding lines are shown in gold and the present-day continental shelf area (excluding floating ice) is marked with black contour lines. Present-day reference topography (BedMachine v3) including basin numbers is shown in panel (c). Yellow and magenta rectangles indicate the Amundsen Sea, see Fig. 4, and Totten region, see Fig. 5, respectively.

in Antarctica contributed with around $15\,\mathrm{m}$ to the global mean (baystatic) sea-level fall of $93\,\mathrm{m}$ at $15\,\mathrm{kyr\,BP}$ ($130\,\mathrm{m}$ during northern hemisphere LGM around $26\,\mathrm{kyr\,BP}$).

230   Variations in the RSL pattern can be ascribed to barystatic, rotational, gravitational, or deformational processes. Hereafter, we will refer to changes in the *far-field*, encompassing those arising from both barystatic effects and all GIA-induced alterations in the northern hemisphere that impact the southern hemisphere. This includes primarily the rotational component and alterations in ocean basin volume due to bedrock deformation linked to changes in ice load. In contrast, we categorize *near-field* effects as RSL changes resulting from GIA processes specific to the Antarctic Ice Sheet, primarily involving gravitational

235   and deformational influences.

The change in sea level relative to present-day as inferred from our coupled ice sheet – GIA model is shown in Fig. 2 for different scenarios. In the *LGM15k* scenario (Fig. 2a) the GIA response to greater ice extent overcompensates the far-field sea-

level fall in many parts: most of West-Antarctica, the Filchner–Ronne and Ross basins and parts of the Peninsula show a total RSL increase, which can mount to +400 m locally. This is also a consequence of the regionally weak Earth structure due to very

240 low mantle viscosities and a thin lithosphere, which is represented in the 3D Earth structure used as input to VILMA (Bagge et al., 2021). In contrast, the *LGM15k* far-field sea-level fall dominates the RSL pattern in all regions of East Antarctica. Locally this RSL pattern is dampened through visco-elastic GIA effects, for instance in the Amery (basin 6) or Totten region (basin 8). The increased ice load leading to bedrock subsidence also causes a displacement of mantle material into the surrounding areas as part of the forebulge effect, which includes the elastic response of the lithosphere. This combined process further reduces

245 the relative sea level in those areas.

In the *icefree* scenario, melting of all ice masses causes a barystatic sea-level rise of +70 m in our simulations and strong bedrock uplift in all previously glaciated regions in both hemispheres. The solid Earth response causes uplift (RSL decrease) of up to 800 m in the interior of the AIS (Fig. 2b). As the mantle material is drained from the surroundings, bedrock subsidence causing an inverse forebulge effect, the RSL increases approx. 20 m more than the far-field sea-level rise in many places of

250 the present-day continental shelf. Areas where the far-field increase in sea level and the near-field bedrock uplift compensate each other (zero contour line of RSL change, dashed) are found close to present-day grounding lines. Results for the *yr2300* scenario are presented in Sec. 3.4.

3.2 Changes in critical access depth

In order to analyse the impact of relative sea-level changes on the access of open ocean water onto the continental shelf, we

255 compute basin-wide critical access depths as explained in Section 2.2 and use bedrock topography, which has been updated with respect to the geoid of the respective scenario presented above (Sec. 3.1).

Present-day critical access depths reveal prominent oceanic gateways (Nicola et al., 2023b, subm.), e.g. in the Filchner–Ronne basin (1) and the Amery basin (6). This can be inferred from Fig. 3a, where the additional colorbar markers (indicating 30 %, 50 % and 70 % of grounding-line accessibility, respectively) are placed at same depths (orange bars represent present-

260 day). Here, large parts of the basin are filled with water of the same critical depth level, due to the retrograde slope with over-deepened bathymetry within the ice-shelf cavity. In the Filchner–Ronne basin more than 75 % of the grounding line is reached by water masses that overflow the topographic sill in 600 m depth. In Amery basin this threshold is at 530 m depth. We identify oceanic gateways also for the Ross (basin 12) and the Amundsen Sea basin (no. 14), where at the deepest open-ocean connection (-570 m and -600 m respectively) 30 % of present-day grounding lines are directly reached.

265 Figure 3a also shows critical access depths calculated for relative sea-level changes in the above defined scenarios, and how they differ from present-day depth (panel b). In the *LGM15k* scenario, barystatic sea level is about 93 m lower than today, which in first estimate would raise critical access depths in all basins, when only the far-field sea-level change with some distance to the AIS was to be considered. This is indicated by a dotted horizontal line in Fig. 3b. Deviations from this line are caused by regional visco-elastic deformations of the lithosphere and mantle and also by the resulting changes in the gravity

270 potential due to mass redistribution and polar motion, all resulting from changes in ice loading.
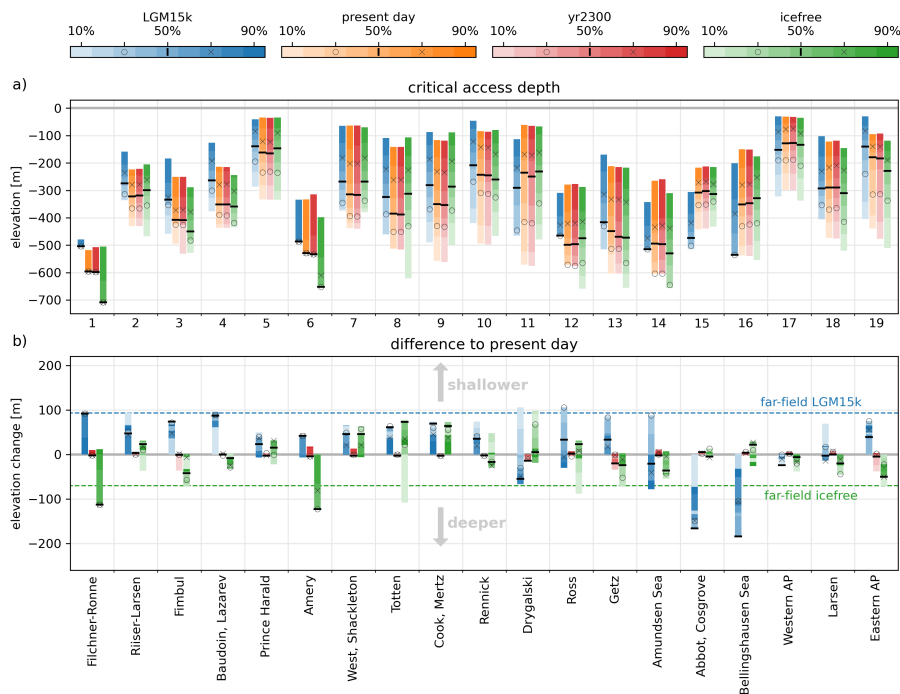
Figure 3. Critical access depths (a) and their changes compared to present-day (b). The colour shade indicates the percentage of grounding line reached by the specific critical access depth, with additional marks at 30 % (**o**), 50 % (**–**) and 70 % (**x**). Barystatic sea-level changes are indicated by dashed horizontal lines in panel b) for *LGM15k* and *icefree* scenario. Basins are labelled according to prominent ice shelves following Nicola et al. (2023b, subm.; with AP = Antarctic Peninsula).

As the concept of critical access depth relates to the potential access of the grounding line, an estimated shift of critical access depths for given changes in relative sea level is not trivial. It depends on a combination of several factors associated with the horizontal fingerprint of relative sea-level changes, which affects the local bedrock depth and its slope angle (retro- or prograde slope), as well as the position and depth of the grounding line. Figure 4 shows this exemplarily for the Amundsen

275 Sea region (basin 14) in the *LGM15k* scenario, where a relatively shallow sill at the front of the continental shelf hinders water masses to reach deeper regions further inland including the present-day grounding line. Relative sea-level change at the outer regions of the continental shelf is dominated by the far-field sea-level change, which reduces the sill depth in the *LGM15k* scenario (meaning the sill is getting shallower). In contrast, relative sea level increases by several hundred meters in the interior of the ice-shelf basin due to increased ice loading and subsidence of the bedrock, counteracting the far-field sea-level fall. These

280 two opposed signals of relative sea-level change can also be observed in the schematic of the Filchner Trough in Fig. 1 (cyan line). Despite the clear pattern of RSL changes in the Amundsen Sea region (Fig. 4b), the horizontal fingerprint of access-depth changes is very heterogeneous (Fig. 4d): it is generally dominated by the sea-level drop at the sill, while bedrock subsidence
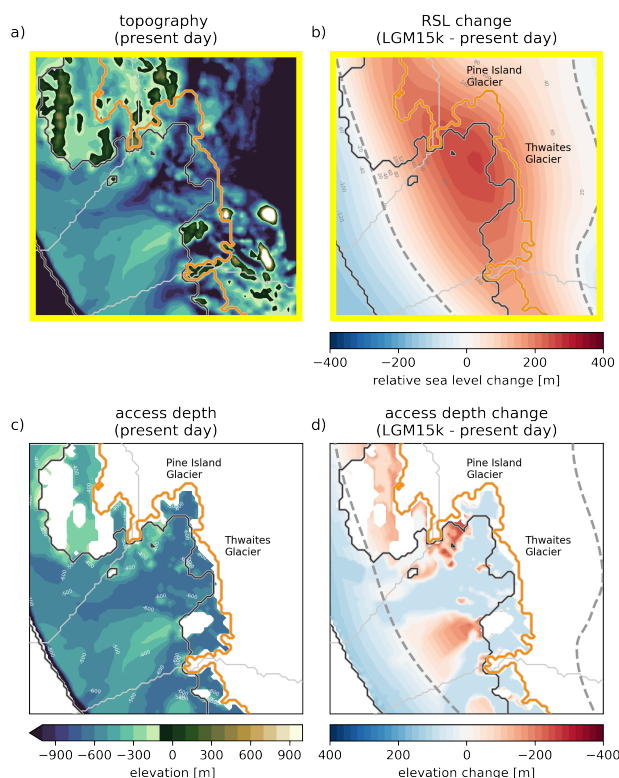
Figure 4. Influence of relative sea-level change on critical access depths in the Amundsen Sea for the *LGM15k* scenario. Upper row shows present-day topography (a) and the change in relative sea level in the *LGM15k* scenario (b). Lower panels show the derived access depths for present-day bathymetry (c) and the corresponding change in the *LGM15k* scenario (d). Horizontally adjusted grounding line for present-day ice distribution is shown in orange and the present-day continental shelf area (excluding floating ice) is marked with black contour lines. The zero contour line of RSL changes is marked as a grey dashed line. Yellow boarders refer to map extent highlighted in Fig. 2.

has no additional effect in the over-deepened interior. A lowering of the access depth only occurs in regions, where present-day topography is higher than the overflow sill (compare Fig. 4a, c and d).

285   In order to determine *critical access depths*, which are defined as one value per basin, the distribution of the horizontally varying *access depths* (see Fig. 4c), in particular at the grounding line, becomes a decisive factor. For comparability we use a grounding line position corresponding to the present-day ice thickness for all scenarios, which has been horizontally adjusted to obtain the floatation criterion for applied bedrock changes. In the *LGM15k* scenario this means for the Amundsen Sea basin that the deepest 45 % of the grounding line is accessed by shallower ocean water compared to present (up to +88 m in elevation)

290 as a result of the far-field decrease in sea level. Shallower parts of the grounding line are instead reached by deeper waters compared to the reference (up to -78 m) as these regions are subject to bedrock subsidence (see Fig. 4b and 3d). This enhances the "oceanic gateway feature" drastically in the sense that a bigger share of the grounding line is reached at lowest possible

overflow depth: in the *LGM15k* case, a vast amount of the entire grounding line (65 %) is reached instantly at an overflow depth of -515 m, whereas the lowest connection at present-day is reaching 30 % of the grounding line (at -603 m, compare blue and orange bars in Fig. 3a, basin 14).

Generally, basins that exhibit an overall RSL fall and have negligible bedrock subsidence show shallower critical access depths in the *LGM15k* scenario compared to present day. This is the case for the entire East Antarctic Ice Sheet (basins 2–10) and the Getz basin (no. 13) in West Antarctica (compare Fig. 2a and 3b). The maximum increase in critical access depths is lower than the far-field sea-level fall in most cases, because the near-field sea-level effects reduce that signal locally. In basins where local bedrock subsidence actually exceed the far-field sea-level signal, critical access depths can be lower and could allow for deeper water masses reaching the grounding lines. This is the case for Ross basin (no. 12) and Drygalski (no. 11) and most of the rest of the West Antarctic Ice Sheet including the Western Antarctic Peninsula (basin 14–17). Despite strong bedrock subsidence being a necessary factor for deeper critical access depths, it is not necessarily a sufficient one. In the Filchner–Ronne basin (no. 1) the whole grounding line is located in a region where GIA-induced bedrock subsidence overcompensates *LGM15k*'s barystatic sea-level lowstand (Fig. 2a). Nevertheless, critical access depths are uniformly shallower in the *LGM15k* scenario (for all grounding line percentages, see Fig. 3b), as the RSL signal at the overflow sill in the outer continental-shelf region is dominated by the far-field sea-level fall and the visco-elastic forebulge effect.

Also in the *icefree* scenario, bedrock topography is a decisive factor to determine the effect of RSL change on critical access depth. Totten Glacier in East Antarctica, for example (basin 8), has deeper access depths compared to present day, despite its grounding line being located in a region which is subject to bedrock uplift caused by ice unloading (see Fig. 5d). As the grounding line depth is much deeper than the overflow sill at the continental-shelf margin, the uplift in the grounding line region has no direct effect on the inferred access depth, and the far-field rise in sea level remains the dominating mechanism. In other parts of the basin, east and west of Totten Glacier, where the grounding-line depth is at a similar elevation or even higher than the sill depth at the continental-shelf margin, the uplift raises the access depths at the grounding line. This explains the strong decrease of critical access depths for the lowest 10 % of the grounding line (-110 m) and an increase for the rest (see Fig. 3 and Fig. 6a). The influence of bedrock uplift (at the present-day grounding line position) is important for the Ross sector (basins 11 & 12) and the Bellingshausen Sea (basin 16) and in some basins of East Antarctica (no. 2, 5, 7-10). Many of these basins show competing effects of far-field sea-level rise and bedrock uplift on the estimate of critical access depth: While the deepest parts of the grounding line, below the sill depth, are mostly affected by the far-field sea-level rise, the shallower portions of the grounding line may be influenced by local bedrock uplift and other near-field GIA effects. This explains why in some cases for an increasing percentage of the grounding line reached, changes of critical access depth switch from a deepening to a shallowing signal. For some basins the so-called "forebulge collapse" is important, where in the surrounding of bedrock uplift the drained mantle material causes a reverse signal (increase in RSL), adding to the far-field rise of sea level. This explains critical access depths reducing even more than the far-field signal (e.g. Filchner–Ronne, Amery or Totten basin, see Fig. 3b).
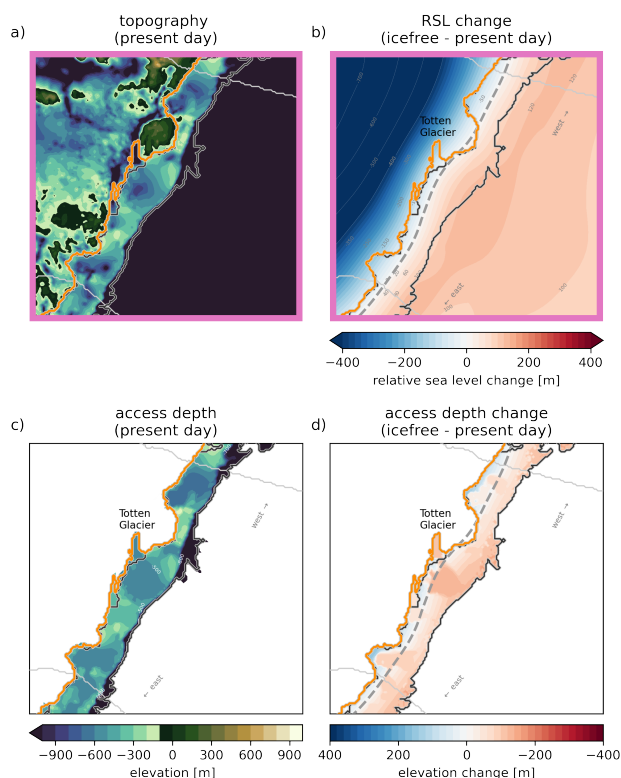
Figure 5. Influence of relative sea-level change on critical access depths in the Totten basin for the *icefree* scenario. Upper row shows present-day topography (a) and change in relative sea level in the *icefree* state (b). Lower panels show the derived access depths for present-day bathymetry (c) and the corresponding change in the *icefree* scenario (d). Horizontally adjusted grounding line is shown in orange and the present-day continental shelf area (excluding floating ice) is marked with black contour lines. The zero contour line of RSL changes is marked as a grey dashed line. Magenta boarders refer to map extent highlighted in Fig. 2.

3.3 Induced changes in ocean properties and sub-shelf melt

In general, the thermocline layer is characterised by steep temperature and salinity gradients with depth. The typical vertical profile of ocean potential temperatures at the continental-shelf break shows a strong increase from about $-1.5\,°C$ at the surface to about $0.5\,°C$ at $600\,m$ depth (see Fig. S4). Below, it decreases slowly with depth to reach about $0\,°C$ at $1800\,m$. Similarly, ocean salinities increase from about $34.0\,psu$ at the surface to ca. $34.7\,psu$ at $600\,m$ depth and stay rather constant below (see Fig. S5). Changes in critical access depth within the thermocline layer can be associated with colder and fresher water when moving upwards in the water column, and warmer, saltier water downwards. Temperature and salinity gradients can differ significantly among basins.

In the *LGM15k* scenario, the implied potential change of present-day temperatures at the continental-shelf break is mostly in the range of $\pm0.5\,°C$ with extreme values up to $\pm0.7\,°C$, see Fig. 6b. Maximum changes of salinities are in the range
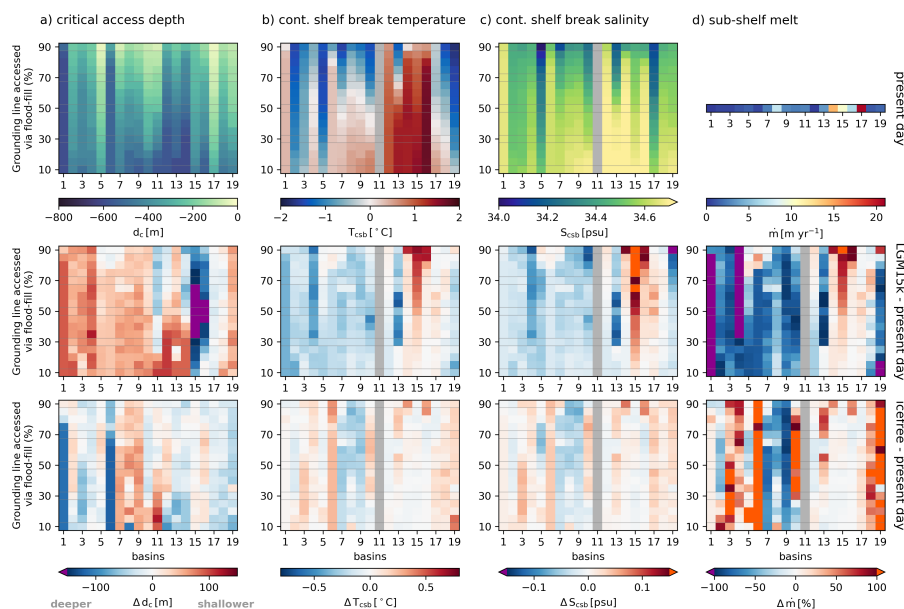
Figure 6. Overview of derived critical access depths, ocean temperatures, salinities and basal melt rates for present-day conditions and their changes in the *LGM15k* and *icefree* scenarios. Results are shown for all 19 Antarctic basins (see Fig. 2c) and grounding line coverage ranging from 10 % to 90 %. Present-day melt rates are computed as in Reese et al. (2023) based on continental-shelf observations of ocean temperature and salinity. Displayed ranges for comparing *LGM15k* and *icefree* conditions to present-day are ±150 m, ±0.8 °C and ±0.15 psu with exceeding values marked with purple and bright red colors respectively.

335 of -0.21 psu to +0.16 psu (Fig. 6c). In almost all of East Antarctica and also the eastern part of the Antarctic Peninsula, temperatures and salinities decrease due to the shallower critical access depth (dominated by far-field sea-level fall). This causes a drastic decrease in basal melt rates, mostly of 50 % or more. In the Filchner–Ronne basin (no. 1) and Baudoin–Lazarev basin (no. 4) this cooling effect is strong enough to support more refreezing underneath the ice shelves than ice-shelf melting, such that on average, the integrated basal mass flux, becomes negative. In West Antarctica (basins 14–16), in contrast, basal

340 melt rates increase significantly, up to a doubling of present-day reference values, which is caused by a deepening of critical access depths. In the Ross basin (no. 12) the sign of effective basal melt rate depends on the portion of accessed grounding line. It ranges from a basal melt decrease (max. −35 %) to an increase (max. +20 %) when grounding line coverage of more than 60 % is considered. This is due to the previously discussed competing effects of far-field sea-level rise and bedrock uplift, which differs between the different depths of grounding line coverage considered (see Sec. 3.2).

345 The *icefree* scenario shows a maximum difference of ±0.5 °C in continental-shelf break temperatures and a range from ±0.08 psu in salinities to the present-day reference, but most values are in the range of ±0.3 °C and ±0.05 psu. A reduction in ocean temperatures and salinites occurs where the bedrock uplift is dominant over the far-field sea-level rise, which is most pronounced in basins 7–9 (East Antarctica). As a result, the melt rates reduce significantly from present-day values of 2.6, 7.2 and 2.9 m yr⁻¹ by -81 %, -75 % and -96 % at maximum (for basins 7–9, respectively). In other regions, however, where
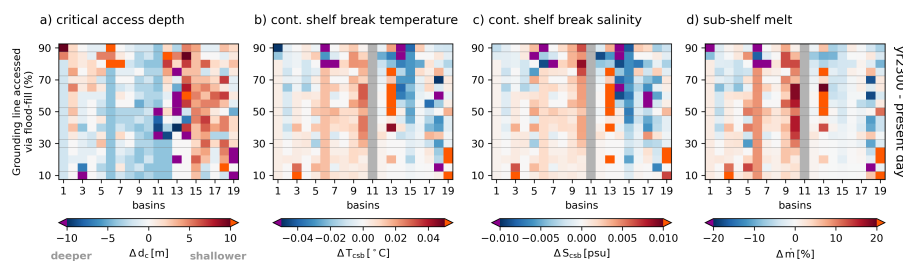
Figure 7. Overview of critical access depth, ocean temperature, salinity and basal melt rate changes in the *yr2300* scenario. Results are shown for all 19 Antarctic basins (see Fig. 2c) and grounding line coverage ranging from 10 % to 90 %.

far-field sea-level rise dominates the RSL signal, a rise in local temperatures and salinities results in strong increase of basal melt rate. This is especially the case in some East Antarctic basins (no. 3, 4, 6 and 10), as well as along the Antarctic Peninsula (basins 17-19), where basal melt rates can double or even triple (maximum 3.6-fold increase) compared to present-day values.

The *icefree* scenario also shows the important influence of critical access depth with respect to the thermocline depth and vertical gradients: Critical access depth drops by ca. 110 m (at grounding line coverage below 75 %) in the Filchner-Ronne basin (no. 1), due to the far-field sea-level increase. However, this has basically no effect in temperature and salinity ($<0.02\,^\circ$C and <0.01 psu) as the present-day critical access depth at approx. -600 m is located below the transition zone, where temperatures and salinities show much lesser gradients with depth (see Fig. 1 and Fig. S4). In other basins, small changes in critical access depths can induce rather large changes in temperature and melt, when the thermocline gradient at access depth is strong: in the Getz basin (no. 13) a decrease of critical access depths by -22 m causes an increase of ocean temperature forcing of $0.23\,^\circ$C which results in an increase of basal melt rate by 72 % (for 80 % grounding line coverage).

3.4 Impact in *yr2300* scenario

In order to assess the impact of relative sea-level changes on sub-shelf melt rates also on centennial time scales, we have included a scenario in the analysis, which reflects an upper limit climate forcing scenario until the year 2300.

The far-field RSL increase in the Southern Ocean around the Antarctic continent is mostly in the range of 4–5 m in the *yr2300* scenario (Fig. 2d). Bedrock uplift caused by grounding line retreat and ice sheet thinning reduces the depth of the water column, in locally strongly differing magnitudes. In regions of strong uplift like in the West Antarctic basins (no. 13–15), the Antarctic Peninsula (no. 16–19), the Filchner–Ronne basin (no. 1) and the Siple Coast in the Ross basin (no. 12), relative sea level is lowered by up to -19 m, overcompensating the far-field sea-level rise. The far-field signal is dominant in large parts of East Antarctica, with some exceptions, like in Dronning Maud Land (basins 2–4), the Amery basin (no. 6) or the Totten glacier (basin 8).

We expect shallower critical access depths compared to the present-day reference mostly in the West-Antarctic basins (no. 14–16), with a maximum depth increase of +11 m in these basins, which correspond to a decrease in temperature up to -0.07 $^\circ$C and -0.02 psu in salinity. In East Antarctica, where the increase in far-field sea-level rise dominates, critical access depths

decrease mostly up to -4 m, which leads to an increase of marginal ocean temperatures and salinities of up to +0.03 °C and
375 +0.009 psu, respectively. Shallower critical access depths for upper grounding line percentages (≥80 %), as found in basins
5–7, are artefacts, which are further explained in the discussion below (Sect. 4). While the bedrock uplift in Dronning Maud
Land (basins 2–4) is reflected in a shallowing of critical access depths and an associated decrease of basal melt for higher
grounding line coverage (≥40 %), this is not observed in Totten basin (no. 8), which also shows an overall RSL reduction
locally.

380   Sea-level induced changes on mean melt rates for East Antarctica increase by up to 20 % compared to present, while they
decrease by up to 10 % in most of West Antarctica (except for basin 13, Getz). This is a relevant but much smaller effect than
the changes induced by climate change as expected in the upcoming centuries, e.g. with an average increase of basal mass
balance by +450 % projected until 2300 by Greve et al. (2023), or the 13-fold increase of mean basal melt rate in Mathiot and
Jourdain (2023, in discus.).

4   Discussion
385

In this section we will critically review the methods we used to derive our results, discuss possible limitations and give context
to the results. Some important points have already been addressed in Nicola et al. (2023b, subm.), as the dependence of the
results on the sub-shelf melt parameterisation (Burgard et al., 2022), the chosen melt parameters for the PICO model or the
influence of basin boundaries. Below, we explain which processes we have considered as static in our analysis such as ice-sheet
390 geometry, ocean dynamics and geomorphology, and discuss other important aspects like data resolution and model parameters.

     To estimate sub-shelf melt changes on paleo time scale scenarios, we use **present-day ocean observations** as the basis for
our analysis, despite the AIS surrounding ocean conditions will likely change considerably on these time scales. The dynamics
of the Southern Ocean, where warm deep waters rise up to intermediate depths, are strongly influenced by local climatic condi-
395 tions as wind patterns, precipitation and air temperature forcing (Rintoul, 2018). Also the processes that regulate the transport
of warm offshore waters onto the continental shelf and towards grounding lines are inherently complex and governed by many
factors: e.g. topographic features, strength and location of sea ice formation, freshwater input through basal melting or tides;
see Thompson et al. (2018) for a detailed review. How oceanic heat supply to AIS margins operates at a variety of spatial and
temporal time scales is described in Colleoni et al. (2018). Models that represent these processes in sufficient resolution are
400 currently actively developed and come at huge computational costs (Pelletier et al., 2022). So including changes of marginal
ocean properties and cross-shelf exchange lies beyond the scope of the study. Instead, we add the RSL induced changes in
ocean properties at the continental-shelf break as anomalies to present-day ocean forcing located inside the ice-shelf cavities. It
is thus possible to differentiate between ocean forcing changes that are due to RSL related geometric shifts and complementary
climatic changes of continental shelf ocean properties.

405

For our analysis, we use present-day bed topography data from Bedmachine v3, which we conservatively regridded from the native **resolution** (500 m) to 8 km horizontally. Nicola et al. (2023b, subm.), who use the data at original resolution, find considerable higher critical access depths for present-day, especially towards higher grounding line coverages, which is caused by substantial higher grounding line depths in the finer dataset. Nevertheless, we do not assume that the resolution effects the

410 overall results of the study.

In our study, we have not considered any **geomorphologic processes** so far. We derive critical access depths through analysing the deepest possible topographic connections between the open ocean and Antarctic grounding line positions. The bedrock on the continental shelf is in many places strongly characterised by troughs and sills, which often determine the access

415 to grounding lines. These topographic features have been formed by previous glacial ice streams and can be in the order of hundreds of meters deep. For example, large gateway-like bed structures were eroded during the last glacials, such as the Filchner Trough or Glomar Challenger Basin in the Ross region, see Nicola et al. (2023b, subm.). For paleo ice-sheet simulations, the representation of erosion and sediment transport (Damsgaard et al., 2020) can have an additional control on sub-shelf melt estimates, as we have only considered present-day topography in our analysis. However, the horizontal resolution and precise

420 location modelled by sedimentary models is key for correctly representing the effect of changing topographic features and the subsequent impact on ice-shelf basal melt rates.

The RSL changes for the different scenarios were informed by coupled PISM-VILMA simulations, which account for the **three-dimensional structure of the Earth**, including laterally varying lithosphere thickness and mantle viscosity (Albrecht

425 et al., 2023, in prep.). A thinner lithosphere and low mantle viscosities, as likely dominant in West Antarctica (Bagge et al., 2021), supports a larger ice-sheet extent (sea-level relevant Antarctic ice volume can be a few meters larger) and much stronger bedrock subsidence (of the order of 100s of meters). In our analysis of critical access depth, the uncertainty in 3D Earth structure hence mainly affects the grounding line depth, but it can also have a significant influence on the forebulge (order of 10s of meters) and hence on critical access depths.

430

In our analysis we consider RSL changes from previously performed coupled ice sheet – GIA model simulations with an evolving ice sheet and grounding line geometry in Antarctica. We then compute and compare RSL-induced changes in ice-shelf basal melt rates with respect to present-day melt rates and ocean conditions, while assuming the same **present-day ice sheet configuration** for all scenarios. This assumption is helpful, as the size, geometry and position of ice shelves alone already influences the local patterns and total amount of basal melting, even with fixed oceanic boundary conditions (De Rydt

435 and Naughten, 2023, in discus.). In case of a major relocation of grounding lines, as for instance at the Last Glacial Maximum, with grounded ice-sheet extent to the edge of the continental shelf, would induce large changes in critical access depths, even if the effect of sea level change was not considered. This is a consequence of the heterogeneous topography structure across the continental shelf, which affects grounding line depths. And apparently, for an *icefree* scenario, there would be no grounding

440   lines or ice shelves left to compute sub-shelf melt rates from. In order to assess the RSL impact on ice-shelf basal melt rates independently from other processes, we use the same ice-sheet geometry for all sea-level scenarios in our assessment.

    The grounding line position is determined by the local ice thickness and the relative sea level. For the present-day ice-sheet geometry and the different RSL change patterns, we do let the **grounding line position adjust** to associated changes in bedrock topography, as a static re-evaluation of the floatation criterion, while we neglect the ice-dynamical adjustment to this

445   change in boundary conditions. This horizontal grounding line adjustment corrects for inconsistent grounding line elevation after applying changes in RSL, which would bias the derived critical access depths. A re-computation of the floatation criterion tends to mitigate the resultant critical access-depth changes by up to $\pm100\,$m for the *LGM15k* and *icefree* scenarios. This is shown in Fig. S6 by a comparison of critical access depths with and without re-adjusting the horizontal grounding line position. A repeated analysis with the non-adjusted critical access depths shows the same pattern of basal melt changes, but with slightly

450   greater magnitude (see Fig. S7).

    The adjustment of the grounding line causes other issues, as for instance additional **noise in the evaluation of critical access-depth changes**. In some cases the adjustment leads to small horizontal shifts in the grounding line of only a few grid cells, which changes the total number of grounding line cells in that basin. When the rest of the grounding line remains unchanged, grounding line coverage of a certain segment can change within a few percent, resulting in jumps of critical access

455   depth, even when the same access depth map (no RSL changes) is evaluated. This is the cause of artefacts that we especially observe in the *yr2300* scenario, where the RSL signal is much smaller compared to the *icefree* or *LGM15k* realisation; and also much smaller than the spatial variability in bed elevation within one grid cell distance (see Fig. S6g, basin 3 and 6, where the unrealistic jumps of -35 m and +22 m occur for example). We expect this noise to be reduced when running the analysis on a finer horizontal resolution. As the horizontal grounding line adjustment is less relevant for small RSL changes, it might be

460   ignored for the *yr2300* scenario. The result of the repeated analysis can be found in the supplementary Fig. S8, which shows a much clearer and de-noised pattern of basal melt rate changes between West (decrease) and East Antarctica (increase) in the range of $\pm20\,\%$.

    The analysis is conducted for a range of **grounding line coverage** reaching from $10\,\%$ to $90\,\%$, which indicates the ground-

465   ing line fraction reached by a specific critical access depth in each basin. As shown in Nicola et al. (2023b, subm.), the deepest grounding line segments typically correlate with fast flowing ice streams regions. According to the overturning circulation modeled by PICO, which is supplied by near-ground inflowing water into the ice-shelf cavities, ocean property changes at low grounding line coverages (e.g. $\leq 30\,\%$) would already have a major influence on the overall basal melt rates. The other ice-shelf regions, away from the fast-flowing ice streams, generally exhibit shallower grounding lines, which require higher grounding

470   line coverage values (e.g. $\geq 70\,\%$) to be reached. These lateral margins exert a buttressing force and decelerates flow dynamics of upstream grounded ice (Reese et al., 2017). Feldmann et al. (2022) show in an idealised setup with prescribed sub-shelf melt rates that melting at shear margins is more effective than in ice-stream locations. Due to the design of our study, which follows an indirect approach of translating offshore water mass changes to grounding line inflow, the grounding line coverage remains as an unconstrained parameter. In general, the inferred range of critical access depths and melt to grounding line coverage in

475 one basin is smaller than the range among different basins.

Our analysis shows that the influence of RSL on ocean forcing ($\pm 1\,°C$ on paleo time scales) is of comparable magnitude as the influence of several other relevant processes. First, the blocking or modification of warm water masses before reaching ice-sheet grounding lines: the observed difference of ocean temperatures at the continental shelf break and inside the ice-shelf
480 cavities is up to $3\,°C$ for present-day (Nicola et al., 2023b, subm.). Second, projected changes of ice-shelf ocean forcing: Naughten et al. (2021) show with high-resolution coupled ocean-ice simulations that a switch from a 'cold' to a 'warm' cavity could happen within the next century under a strong climate warming scenario, which would increase temperature forcing by about $2\,°C$ in the Filchner–Ronne basin. And third, the range of offshore ocean thermal forcing on glacial time scales: during glacial climates, we assume that ocean temperatures, used as input for PICO, were cooled down at the surface and are hence
485 bounded below by the surface pressure melting point (about $-1.9\,°C$), which is 0.2–$3.1\,°C$ below present-day temperature observations in the different basins (Reese et al., 2018, Fig. 2), marking the lower limit of ocean thermal forcing.

From various ice-sheet simulations we know that already $1\,°C$ of warming can have large impacts on sub-shelf melting and ice-sheet dynamics, in particular close to tipping thresholds. Thus, the interaction of ocean, sea-level and solid Earth processes, in some Antarctic basins, may contribute significantly to enhanced sea-level rise with impacts on future societies.

490 ## 5 Conclusions

In our study we evaluate the potential effects of geometric changes in the water column thickness on ice-shelf basal melt, governed by changes in relative sea level. We compare our estimates to similar effects induced by shifts in climatic boundary conditions, associated with altered wind patterns, sea ice and ocean dynamics. Our analysis shows that relative sea-level changes in the order of 100 meters can induce changes of sub-shelf melting in the range of $\pm 100\,\%$ as a consequence of warm
495 Circumpolar Deep Water intrusions onto the continental shelf and into ice-shelf cavities. The relevancy of this process is bound to the time scales of global sea-level changes and GIA response and fully unfolds over paleo time scales. We recommend to consider the influence of relative sea level on ocean forcing for millennial scale simulations of the Antarctic Ice Sheet. In fact, we estimate significant changes in ice-shelf basal melt rates of $\pm 20\,\%$ already within the next three centuries, which could have important implications for projections of Antarctic ice losses and associated contributions to global sea-level rise.

500 *Code and data availability.* The data and relevant code will be made publicly available on a public data repository i.e. PANGAEA or Zenodo. DOI links to the repositories will be provided upon publication

Author contributions. RW and TA conceptualized the study, whereas MK, TA and LN developed the detailed study methodology. MK, TA and LN carried out the analysis and TA contributed the PISM-VILMA simulations. RR provided the PISM-PICO setup. RW, RR and LN

co-developed the oceanic gateway methodology. MK wrote the manuscript and prepared the figures, with contributions from LN. All authors
contributed to the final version with input and suggestions.

Competing interests. The authors declare that they have no competing interests.

Acknowledgements. This work was supported by the Deutsche Forschungsgemeinschaft (DFG) in the framework of the priority program
SPP 1158 "Antarctic Research with comparative investigations in Arctic ice areas" by the following grant: WI 4556/4-1. MK was financially
supported by the Potsdam Graduate School. The work of TA and RW has been conducted within the framework of the PalMod project
(grant no. FKZ: 01LP1925D, 01LP2305B), supported by the German Federal Ministry of Education and Research (BMBF) as Research for
Sustainability initiative (FONA). TA and RW acknowledge support by OCEAN:ICE, which is co-funded by the European Union, Horizon
Europe Funding Programme for research and innovation under grant agreement Nr. 101060452 and by UK Research and Innovation. O:I
Contribution number 2. LN was supported by the Studienstiftung des Deutschen Volkes (German National Academic Foundation). MK,
LN, RR and RW gratefully acknowledge support by the European Union's Horizon 2020 research and innovation programme under Grant
Agreement No. 820575 (TiPACCs). RW further acknowledges support by the European Union's Horizon 2020 under Grant Agreement
No. 869304 (PROTECT). Development of PISM is supported by NASA grants 20-CRYO2020-0052 and 80NSSC22K0274 and NSF grant
OAC-2118285. The authors gratefully acknowledge the European Regional Development Fund (ERDF), the German Federal Ministry of
Education and Research and the Land Brandenburg for supporting this project by providing resources on the high performance computer
system at the Potsdam Institute for Climate Impact Research.

References

520

Albrecht, T., Winkelmann, R., and Levermann, A.: Glacial-cycle simulations of the Antarctic Ice Sheet with the Parallel Ice Sheet Model (PISM) – Part 1: Boundary conditions and climatic forcing, The Cryosphere, 14, 599–632, https://doi.org/10.5194/tc-14-599-2020, 2020a.

Albrecht, T., Winkelmann, R., and Levermann, A.: Glacial-cycle simulations of the Antarctic Ice Sheet with the Parallel Ice Sheet Model (PISM) – Part 2: Parameter ensemble analysis, The Cryosphere, 14, 633–656, https://doi.org/10.5194/tc-14-633-2020, 2020b.

525 Albrecht, T., Bagge, M., Winkelmann, R., and Klemann, V.: Stability of the Antarctic Ice Sheet in interaction with the solid Earth, in preparation, 2023.

Bagge, M., Klemann, V., Steinberger, B., Latinović, M., and Thomas, M.: Glacial-Isostatic Adjustment Models Using Geodynamically Constrained 3D Earth Structures, Geochemistry, Geophysics, Geosystems, 22, https://doi.org/10.1029/2021gc009853, 2021.

Barletta, V. R., Bevis, M., Smith, B. E., Wilson, T., Brown, A., Bordoni, A., Willis, M., Khan, S. A., Rovira-Navarro, M., Dalziel, I., Smalley,
530 R., Kendrick, E., Konfal, S., Caccamise, D. J., Aster, R. C., Nyblade, A., and Wiens, D. A.: Observed rapid bedrock uplift in Amundsen Sea Embayment promotes ice-sheet stability, Science, 360, 1335–1339, https://doi.org/10.1126/science.aao1447, 2018.

Bentley, M. J., Cofaigh, C. Ó., Anderson, J. B., Conway, H., Davies, B., Graham, A. G., Hillenbrand, C.-D., Hodgson, D. A., Jamieson, S. S., Larter, R. D., Mackintosh, A., Smith, J. A., Verleyen, E., Ackert, R. P., Bart, P. J., Berg, S., Brunstein, D., Canals, M., Colhoun, E. A., Crosta, X., Dickens, W. A., Domack, E., Dowdeswell, J. A., Dunbar, R., Ehrmann, W., Evans, J., Favier, V., Fink, D., Fogwill,
535 C. J., Glasser, N. F., Gohl, K., Golledge, N. R., Goodwin, I., Gore, D. B., Greenwood, S. L., Hall, B. L., Hall, K., Hedding, D. W., Hein, A. S., Hocking, E. P., Jakobsson, M., Johnson, J. S., Jomelli, V., Jones, R. S., Klages, J. P., Kristoffersen, Y., Kuhn, G., Leventer, A., Licht, K., Lilly, K., Lindow, J., Livingstone, S. J., Massé, G., McGlone, M. S., McKay, R. M., Melles, M., Miura, H., Mulvaney, R., Nel, W., Nitsche, F. O., O'Brien, P. E., Post, A. L., Roberts, S. J., Saunders, K. M., Selkirk, P. M., Simms, A. R., Spiegel, C., Stolldorf, T. D., Sugden, D. E., van der Putten, N., van Ommen, T., Verfaillie, D., Vyverman, W., Wagner, B., White, D. A., Witus, A. E., and Zwartz, D.:
540 A community-based geological reconstruction of Antarctic Ice Sheet deglaciation since the Last Glacial Maximum, Quaternary Science Reviews, 100, 1–9, https://doi.org/10.1016/j.quascirev.2014.06.025, 2014.

Bueler, E. and Brown, J.: Shallow shelf approximation as a "sliding law" in a thermomechanically coupled ice sheet model, Journal of Geophysical Research, 114, https://doi.org/10.1029/2008jf001179, 2009.

Burgard, C., Jourdain, N. C., Reese, R., Jenkins, A., and Mathiot, P.: An assessment of basal melt parameterisations for Antarctic ice shelves,
545 The Cryosphere, 16, 4931–4975, https://doi.org/10.5194/tc-16-4931-2022, 2022.

Chandler, D., Langebroek, P., Reese, R., Albrecht, T., Garbe, J., and Winkelmann, R.: Antarctic Ice Sheet tipping in the last 800 kyr warns of future ice loss, https://doi.org/10.21203/rs.3.rs-3042739/v1, in review, 2023.

Chandler, D. M. and Langebroek, P. M.: Glacial-interglacial Circumpolar Deep Water temperatures during the last 800,000 years: estimates from a synthesis of bottom water temperature reconstructions, https://doi.org/10.5194/egusphere-2023-850, in review, 2023.

550 Clark, P. U., Dyke, A. S., Shakun, J. D., Carlson, A. E., Clark, J., Wohlfarth, B., Mitrovica, J. X., Hostetler, S. W., and McCabe, A. M.: The Last Glacial Maximum, Science, 325, 710–714, https://doi.org/10.1126/science.1172873, 2009.

Colleoni, F., Santis, L. D., Siddoway, C. S., Bergamasco, A., Golledge, N. R., Lohmann, G., Passchier, S., and Siegert, M. J.: Spatio-temporal variability of processes across Antarctic ice-bed–ocean interfaces, Nature Communications, 9, https://doi.org/10.1038/s41467-018-04583-0, 2018.

555 Coulon, V., Bulthuis, K., Whitehouse, P. L., Sun, S., Haubner, K., Zipf, L., and Pattyn, F.: Contrasting Response of West and East Antarctic
        Ice Sheets to Glacial Isostatic Adjustment, Journal of Geophysical Research: Earth Surface, 126, https://doi.org/10.1029/2020jf006003,
        2021.

Damsgaard, A., Goren, L., and Suckale, J.: Water pressure fluctuations control variability in sediment flux and slip dynamics beneath glaciers
        and ice streams, Communications Earth & Environment, 1, https://doi.org/10.1038/s43247-020-00074-7, 2020.

560 De Rydt, J. and Naughten, K.: Geometric amplification and suppression of ice-shelf basal melt in West Antarctica,
        https://doi.org/10.5194/egusphere-2023-1587, in review, 2023.

Farrell, W. E. and Clark, J. A.: On Postglacial Sea Level, Geophysical Journal of the Royal Astronomical Society, 46, 647–667,
        https://doi.org/10.1111/j.1365-246x.1976.tb01252.x, 1976.

Feldmann, J., Reese, R., Winkelmann, R., and Levermann, A.: Shear-margin melting causes stronger transient ice discharge than ice-stream

565   melting in idealized simulations, The Cryosphere, 16, 1927–1940, https://doi.org/10.5194/tc-16-1927-2022, 2022.

Fox-Kemper, B., Hewitt, H., Xiao, C., Aðalgeirsdóttir, G., Drijfhout, S., Edwards, T., Golledge, N., Hemer, M., Kopp, R., Krinner, G.,
        Mix, A., Notz, D., Nowicki, S., Nurhati, I., Ruiz, L., Sallée, J.-B., Slangen, A., and Yu, Y.: Ocean, Cryosphere and Sea Level Change,
        in: Climate Change 2021: The Physical Science Basis. Contribution of Working Group I to the Sixth Assessment Report of the Inter-
        governmental Panel on Climate Change, edited by Masson-Delmotte, V., Zhai, P., Pirani, A., Connors, S., Péan, C., Berger, S., Caud,

570   N., Chen, Y., Goldfarb, L., Gomis, M., Huang, M., Leitzell, K., Lonnoy, E., Matthews, J., Maycock, T., Waterfield, T., Yelekçi, O., Yu,
        R., and Zhou, B., book section 9, p. 1211–1362, Cambridge University Press, Cambridge, United Kingdom and New York, NY, USA,
        https://doi.org/10.1017/9781009157896.011, 2021.

Garbe, J., Albrecht, T., Levermann, A., Donges, J. F., and Winkelmann, R.: The hysteresis of the Antarctic ice sheet, Nature, 585, 538–544,
        https://doi.org/10.1038/s41586-020-2727-5, 2020.

575 Gebbie, G.: Cancelation of Deglacial Thermosteric Sea Level Rise by a Barosteric Effect, Journal of Physical Oceanography, 50, 3623–3639,
        https://doi.org/10.1175/jpo-d-20-0173.1, 2020.

Gomez, N., Weber, M. E., Clark, P. U., Mitrovica, J. X., and Han, H. K.: Antarctic ice dynamics amplified by Northern Hemisphere sea-level
        forcing, Nature, 587, 600–604, https://doi.org/10.1038/s41586-020-2916-2, 2020.

Gregory, J. M., Griffies, S. M., Hughes, C. W., Lowe, J. A., Church, J. A., Fukimori, I., Gomez, N., Kopp, R. E., Landerer, F., Cozannet,

580   G. L., Ponte, R. M., Stammer, D., Tamisiea, M. E., and van de Wal, R. S. W.: Concepts and Terminology for Sea Level: Mean, Variability
        and Change, Both Local and Global, Surveys in Geophysics, 40, 1251–1289, https://doi.org/10.1007/s10712-019-09525-z, 2019.

Greve, R., Chambers, C., Obase, T., Saito, F., Chan, W.-L., and Abe-Ouchi, A.: Future projections for the Antarctic ice sheet until the year
        2300 with a climate-index method, Journal of Glaciology, pp. 1–11, https://doi.org/10.1017/jog.2023.41, 2023.

Gulev, S., Thorne, P., Ahn, J., Dentener, F., Domingues, C., Gerland, S., Gong, D., Kaufman, D., Nnamchi, H., Quaas, J., Rivera, J.,

585   Sathyendranath, S., Smith, S., Trewin, B., von Schuckmann, K., and Vose, R.: Changing State of the Climate System, in: Climate
        Change 2021: The Physical Science Basis. Contribution of Working Group I to the Sixth Assessment Report of the Intergovern-
        mental Panel on Climate Change, edited by Masson-Delmotte, V., Zhai, P., Pirani, A., Connors, S., Péan, C., Berger, S., Caud, N.,
        Chen, Y., Goldfarb, L., Gomis, M., Huang, M., Leitzell, K., Lonnoy, E., Matthews, J., Maycock, T., Waterfield, T., Yelekçi, O., Yu,
        R., and Zhou, B., book section 2, p. 287–422, Cambridge University Press, Cambridge, United Kingdom and New York, NY, USA,

590   https://doi.org/10.1017/9781009157896.004, 2021.

Hellmer, H. H., Kauker, F., Timmermann, R., Determann, J., and Rae, J.: Twenty-first-century warming of a large Antarctic ice-shelf cavity
        by a redirected coastal current, Nature, 485, 225–228, https://doi.org/10.1038/nature11064, 2012.

Horwath, M., Gutknecht, B. D., Cazenave, A., Palanisamy, H. K., Marti, F., Marzeion, B., Paul, F., Bris, R. L., Hogg, A. E., Otosaka, I.,
Shepherd, A., Döll, P., Cáceres, D., Schmied, H. M., Johannessen, J. A., Nilsen, J. E. Ø., Raj, R. P., Forsberg, R., Sørensen, L. S., Barletta,
595   V. R., Simonsen, S. B., Knudsen, P., Andersen, O. B., Ranndal, H., Rose, S. K., Merchant, C. J., Macintosh, C. R., von Schuckmann, K.,
Novotny, K., Groh, A., Restano, M., and Benveniste, J.: Global sea-level budget and ocean-mass budget, with a focus on advanced data
products and uncertainty characterisation, Earth System Science Data, 14, 411–447, https://doi.org/10.5194/essd-14-411-2022, 2022.

Jones, R. S., Johnson, J. S., Lin, Y., Mackintosh, A. N., Sefton, J. P., Smith, J. A., Thomas, E. R., and Whitehouse, P. L.: Stability of the
Antarctic Ice Sheet during the pre-industrial Holocene, Nature Reviews Earth & Environment, 3, 500–515, https://doi.org/10.1038/s43017-
600   022-00309-5, 2022.

Jourdain, N. C., Asay-Davis, X., Hattermann, T., Straneo, F., Seroussi, H., Little, C. M., and Nowicki, S.: A protocol for calculating basal
melt rates in the ISMIP6 Antarctic ice sheet projections, The Cryosphere, 14, 3111–3134, https://doi.org/10.5194/tc-14-3111-2020, 2020.

Klemann, V., Martinec, Z., and Ivins, E. R.: Glacial isostasy and plate motion, Journal of Geodynamics, 46, 95–103,
https://doi.org/10.1016/j.jog.2008.04.005, 2008.

605   Lambeck, K., Rouby, H., Purcell, A., Sun, Y., and Sambridge, M.: Sea level and global ice volumes from the Last Glacial Maximum to the
Holocene, Proceedings of the National Academy of Sciences, 111, 15 296–15 303, https://doi.org/10.1073/pnas.1411762111, 2014.

Martinec, Z., Klemann, V., van der Wal, W., Riva, R. E. M., Spada, G., Sun, Y., Melini, D., Kachuck, S. B., Barletta, V., Simon, K., A,
G., and James, T. S.: A benchmark study of numerical implementations of the sea level equation in GIA modelling, Geophysical Journal
International, 215, 389–414, https://doi.org/10.1093/gji/ggy280, 2018.

610   Mathiot, P. and Jourdain, N. C.: High-end projections of Southern Ocean warming and Antarctic ice shelf melting in conditions typical of
the end of the 23rd century, https://doi.org/10.5194/egusphere-2023-1606, in review, 2023.

Miller, K. G., Browning, J. V., Schmelz, W. J., Kopp, R. E., Mountain, G. S., and Wright, J. D.: Cenozoic sea-level and cryospheric evolution
from deep-sea geochemical and continental margin records, Science advances, 6, eaaz1346, https://doi.org/10.1126/sciadv.aaz1346, 2020.

Morlighem, M.: MEaSUREs BedMachine Antarctica, Version 3 [dataset], https://doi.org/10.5067/FPSU0V1MWUB6, 2022.

615   Morlighem, M., Rignot, E., Binder, T., Blankenship, D., Drews, R., Eagles, G., Eisen, O., Ferraccioli, F., Forsberg, R., Fretwell, P., Goel,
V., Greenbaum, J. S., Gudmundsson, H., Guo, J., Helm, V., Hofstede, C., Howat, I., Humbert, A., Jokat, W., Karlsson, N. B., Lee, W. S.,
Matsuoka, K., Millan, R., Mouginot, J., Paden, J., Pattyn, F., Roberts, J., Rosier, S., Ruppel, A., Seroussi, H., Smith, E. C., Steinhage,
D., Sun, B., van den Broeke, M. R., van Ommen, T. D., van Wessem, M., and Young, D. A.: Deep glacial troughs and stabilizing ridges
unveiled beneath the margins of the Antarctic ice sheet, Nature Geoscience, 13, 132–137, https://doi.org/10.1038/s41561-019-0510-8,
620   2020.

Naughten, K. A., Rydt, J. D., Rosier, S. H. R., Jenkins, A., Holland, P. R., and Ridley, J. K.: Two-timescale response of a large Antarctic ice
shelf to climate change, Nature Communications, 12, https://doi.org/10.1038/s41467-021-22259-0, 2021.

Nicola, L., Notz, D., and Winkelmann, R.: Revisiting temperature sensitivity: how does Antarctic precipitation change with temperature?,
The Cryosphere, 17, 2563–2583, https://doi.org/10.5194/tc-17-2563-2023, 2023a.

625   Nicola, L., Reese, R., , Albrecht, T., Kreuzer, M., and Winkelmann, R.: Oceanic gateways to Antarctic grounding lines - Impact of critical
access depths on sub-shelf melt, The Cryosphere, submitted, 2023b.

Olbers, D. and Hellmer, H.: A box model of circulation and melting in ice shelf caverns, Ocean Dynamics, 60, 141–153,
https://doi.org/10.1007/s10236-009-0252-z, 2010.

Otosaka, I. N., Shepherd, A., Ivins, E. R., Schlegel, N.-J., Amory, C., van den Broeke, M. R., Horwath, M., Joughin, I., King, M. D., Krinner,
630   G., Nowicki, S., Payne, A. J., Rignot, E., Scambos, T., Simon, K. M., Smith, B. E., Sørensen, L. S., Velicogna, I., Whitehouse, P. L., A,

G., Agosta, C., Ahlstrøm, A. P., Blazquez, A., Colgan, W., Engdahl, M. E., Fettweis, X., Forsberg, R., Gallée, H., Gardner, A., Gilbert, L., Gourmelen, N., Groh, A., Gunter, B. C., Harig, C., Helm, V., Khan, S. A., Kittel, C., Konrad, H., Langen, P. L., Lecavalier, B. S., Liang, C.-C., Loomis, B. D., McMillan, M., Melini, D., Mernild, S. H., Mottram, R., Mouginot, J., Nilsson, J., Noël, B., Pattle, M. E., Peltier, W. R., Pie, N., Roca, M., Sasgen, I., Save, H. V., Seo, K.-W., Scheuchl, B., Schrama, E. J. O., Schröder, L., Simonsen, S. B., Slater, T., Spada, G., Sutterley, T. C., Vishwakarma, B. D., van Wessem, J. M., Wiese, D., van der Wal, W., and Wouters, B.: Mass balance of the Greenland and Antarctic ice sheets from 1992 to 2020, Earth System Science Data, 15, 1597–1616, https://doi.org/10.5194/essd-15-1597-2023, 2023.

Pelletier, C., Fichefet, T., Goosse, H., Haubner, K., Helsen, S., Huot, P.-V., Kittel, C., Klein, F., clec'h, S. L., van Lipzig, N. P. M., Marchi, S., Massonnet, F., Mathiot, P., Moravveji, E., Moreno-Chamarro, E., Ortega, P., Pattyn, F., Souverijns, N., Achter, G. V., Broucke, S. V., Vanhulle, A., Verfaillie, D., and Zipf, L.: PARASO, a circum-Antarctic fully coupled ice-sheet–ocean–sea-ice–atmosphere–land model involving f.ETISh1.7, NEMO3.6, LIM3.6, COSMO5.0 and CLM4.5, Geoscientific Model Development, 15, 553–594, https://doi.org/10.5194/gmd-15-553-2022, 2022.

Pollard, D., Gomez, N., and Deconto, R. M.: Variations of the Antarctic Ice Sheet in a Coupled Ice Sheet-Earth-Sea Level Model: Sensitivity to Viscoelastic Earth Properties, Journal of Geophysical Research: Earth Surface, 122, 2124–2138, https://doi.org/10.1002/2017jf004371, 2017.

Pritchard, H. D., Ligtenberg, S. R. M., Fricker, H. A., Vaughan, D. G., van den Broeke, M. R., and Padman, L.: Antarctic ice-sheet loss driven by basal melting of ice shelves, Nature, 484, 502–505, https://doi.org/10.1038/nature10968, 2012.

Reese, R., Gudmundsson, G. H., Levermann, A., and Winkelmann, R.: The far reach of ice-shelf thinning in Antarctica, Nature Climate Change, 8, 53–57, https://doi.org/10.1038/s41558-017-0020-x, 2017.

Reese, R., Albrecht, T., Mengel, M., Asay-Davis, X., and Winkelmann, R.: Antarctic sub-shelf melt rates via PICO, The Cryosphere, 12, 1969–1985, https://doi.org/10.5194/tc-12-1969-2018, 2018.

Reese, R., Garbe, J., Hill, E. A., Urruty, B., Naughten, K. A., Gagliardini, O., Durand, G., Gillet-Chaulet, F., Gudmundsson, G. H., Chandler, D., Langebroek, P. M., and Winkelmann, R.: The stability of present-day Antarctic grounding lines – Part 2: Onset of irreversible retreat of Amundsen Sea glaciers under current climate on centennial timescales cannot be excluded, The Cryosphere, 17, 3761–3783, https://doi.org/10.5194/tc-17-3761-2023, 2023.

Rignot, E., Mouginot, J., Scheuchl, B., van den Broeke, M., van Wessem, M. J., and Morlighem, M.: Four decades of Antarctic Ice Sheet mass balance from 1979–2017, Proceedings of the National Academy of Sciences, 116, 1095–1103, https://doi.org/10.1073/pnas.1812883116, 2019.

Rintoul, S. R.: The global influence of localized dynamics in the Southern Ocean, Nature, 558, 209–218, https://doi.org/10.1038/s41586-018-0182-3, 2018.

Rintoul, S. R., Silvano, A., Pena-Molino, B., van Wijk, E., Rosenberg, M., Greenbaum, J. S., and Blankenship, D. D.: Ocean heat drives rapid basal melt of the Totten Ice Shelf, Science Advances, 2, https://doi.org/10.1126/sciadv.1601610, 2016.

Rydt, J. D. and Gudmundsson, G. H.: Coupled ice shelf-ocean modeling and complex grounding line retreat from a seabed ridge, Journal of Geophysical Research: Earth Surface, 121, 865–880, https://doi.org/10.1002/2015jf003791, 2016.

Schmidtko, S., Heywood, K. J., Thompson, A. F., and Aoki, S.: Multidecadal warming of Antarctic waters, Science, 346, 1227–1231, https://doi.org/10.1126/science.1256117, 2014.

Shepherd, A., Ivins, E. R., A, G., Barletta, V. R., Bentley, M. J., Bettadpur, S., Briggs, K. H., Bromwich, D. H., Forsberg, R., Galin, N., Horwath, M., Jacobs, S., Joughin, I., King, M. A., Lenaerts, J. T. M., Li, J., Ligtenberg, S. R. M., Luckman, A., Luthcke, S. B., McMillan, M., Meister, R., Milne, G., Mouginot, J., Muir, A., Nicolas, J. P., Paden, J., Payne, A. J., Pritchard, H., Rignot, E., Rott, H., Sørensen,

L. S., Scambos, T. A., Scheuchl, B., Schrama, E. J. O., Smith, B., Sundal, A. V., van Angelen, J. H., van de Berg, W. J., van den Broeke,
M. R., Vaughan, D. G., Velicogna, I., Wahr, J., Whitehouse, P. L., Wingham, D. J., Yi, D., Young, D., and Zwally, H. J.: A Reconciled
Estimate of Ice-Sheet Mass Balance, Science, 338, 1183–1189, https://doi.org/10.1126/science.1228102, 2012.

Stuhne, G. R. and Peltier, W. R.: Reconciling the ICE-6G_C reconstruction of glacial chronology with ice sheet dynamics: The cases of
Greenland and Antarctica, Journal of Geophysical Research: Earth Surface, 120, 1841–1865, https://doi.org/10.1002/2015jf003580, 2015.

The ISMIP6 2300 extension authors: ISMIP6 Projections 2300 Antarctica, https://theghub.org/groups/ismip6/wiki/
ISMIP6-Projections2300-Antarctica, Last accessed July 25, 2023, 2022.

Thompson, A. F., Stewart, A. L., Spence, P., and Heywood, K. J.: The Antarctic Slope Current in a Changing Climate, Reviews of Geophysics,
56, 741–770, https://doi.org/10.1029/2018rg000624, 2018.

van Calcar, C. J., van de Wal, R. S. W., Blank, B., de Boer, B., and van der Wal, W.: Simulation of a fully coupled 3D glacial iso-
static adjustment – ice sheet model for the Antarctic ice sheet over a glacial cycle, Geoscientific Model Development, 16, 5473–5492,
https://doi.org/10.5194/gmd-16-5473-2023, 2023.

Whitehouse, P. L.: Glacial isostatic adjustment modelling: historical perspectives, recent advances, and future directions, Earth Surface
Dynamics, 6, 401–429, https://doi.org/10.5194/esurf-6-401-2018, 2018.

Whitehouse, P. L., Gomez, N., King, M. A., and Wiens, D. A.: Solid Earth change and the evolution of the Antarctic Ice Sheet, Nature
Communications, 10, https://doi.org/10.1038/s41467-018-08068-y, 2019.

Winkelmann, R., Martin, M. A., Haseloff, M., Albrecht, T., Bueler, E., Khroulev, C., and Levermann, A.: The Potsdam Parallel Ice Sheet
Model (PISM-PIK) – Part 1: Model description, The Cryosphere, 5, 715–726, https://doi.org/10.5194/tc-5-715-2011, 2011.

Yokoyama, Y., Esat, T. M., Thompson, W. G., Thomas, A. L., Webster, J. M., Miyairi, Y., Sawada, C., Aze, T., Matsuzaki, H., Okuno, J.,
Fallon, S., Braga, J.-C., Humblet, M., Iryu, Y., Potts, D. C., Fujita, K., Suzuki, A., and Kan, H.: Rapid glaciation and a two-step sea level
plunge into the Last Glacial Maximum, Nature, 559, 603–607, https://doi.org/10.1038/s41586-018-0335-4, 2018.

Zeitz, M., Haacker, J. M., Donges, J. F., Albrecht, T., and Winkelmann, R.: Dynamic regimes of the Greenland Ice Sheet emerging from in-
teracting melt–elevation and glacial isostatic adjustment feedbacks, Earth System Dynamics, 13, 1077–1096, https://doi.org/10.5194/esd-
13-1077-2022, 2022.

Zwally, H. J., Giovinetto, M. B., Beckley, M. A., and Saba, J. L.: Antarctic and Greenland Drainage Systems [Dataset], http://imbie.org/
imbie-3/drainage-basins/, accessed 27 November 2018, 2012.